ACS APPLIED MATERIALS & INTERFACES

Research Article

www.acsami.org

Room Temperature Fabrication of Dielectric Bragg Reflectors Composed of a CaF_2/ZnS Multilayered Coating

Merav Muallem, Alex Palatnik, Gilbert D. Nessim, and Yaakov R. Tischler*

The Department of Chemistry and the Bar-Ilan Institute for Nanotechnology and Advanced Materials, Bar-Ilan University, Ramat Gan 52900, Israel

Supporting Information

ABSTRACT: We describe the design, fabrication, and characterization of mechanically stable, reproducible, and highly reflecting distributed Bragg reflectors (DBR) composed of thermally evaporated thin films of calcium fluoride (CaF_2) and zinc sulfide (ZnS). CaF_2 and ZnS were chosen as the low and high refractive index components of the multilayer DBR structures, with n = 1.43 and n = 2.38 respectively, because neither material requires substrate heating during the deposition process in order to produce optical quality thin films. DBRs consisting of seven pairs of CaF_2 and ZnS layers, were fabricated with thicknesses of 96 and 58 nm, respectively, as characterized by high-resolution scanning electron microscopy (HR-SEM), and exhibited a center wavelength of λ_c = 550 nm and peak reflectance exceeding 99%. The layers showed good adhesion to each other and to the glass substrate, resulting in mechanically stable DBR coatings. Complete optical microcavities consisting of two such DBR coatings and a CaF_2 spacer layer between them could be fabricated in a single deposition run. Optically, these structures exhibited a resonator quality factor of Q > 160. When a CaF_2/ZnS DBR was grown, without heating the substrate during deposition, on top of a thin film containing the fluorescent dye Rhodamine 6G, the fluorescence intensity showed no degradation compared to an uncoated film, in contrast to a MgF_2/ZnS DBR coating grown with substrate heating which showed a 92% reduction in signal. The ability to fabricate optical quality CaF_2/ZnS DBRs without substrate heating, as introduced here, can therefore enable formation of low-loss high-reflectivity coatings on top of more delicate heat-sensitive materials such as organics and other nanostructured emitters, and hence facilitate the development of nanoemitter-based microcavity device applications.

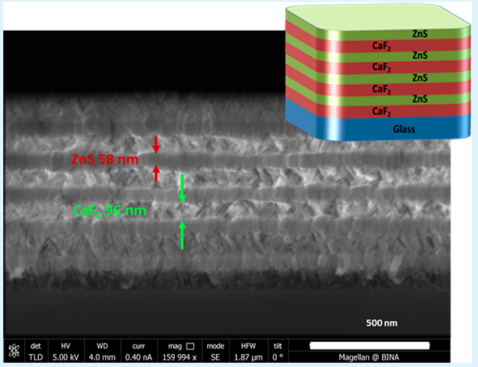

KEYWORDS: *thermal evaporation, DBR, multilayer coating, calcium fluoride, zinc sulfide*

1. INTRODUCTION

A distributed Bragg reflector (DBR) is a mirror-like coating based on dielectric materials. DBRs are commonly incorporated in optical devices such as waveguide lasers and microcavity resonators in order to obtain high reflectivity at a specific center wavelength, λ_c, or over a range of wavelengths centered around λ_c. DBRs are composed of pairs of dielectric materials, with each pair consisting of a high and low refractive index, n_H and n_L, respectively. Please note that the refractive index is in general wavelength dependent. For a given λ_c, the thickness of each layer is chosen to satisfy the "Bragg condition" in analogy to crystal diffraction: $d_i = \lambda_c/4n_i$, which results in constructive interference of the beams that are reflected from each interface and an overall reflectivity, R, that can approach unity. For a DBR, R is given by the following equation:[1]

$$R = \left[\frac{n_0(n_L)^{2N} - n_s(n_H)^{2N}}{n_0(n_L)^{2N} + n_s(n_H)^{2N}}\right]^2 \quad (1)$$

where N is the number of pairs of layers in the stack, and n_0, n_H, n_L and n_s are the respective refractive indices of the originating medium (typically air), the high and low index materials, and the substrate. Increasing the number of layers and/or the index contrast between them will increase the reflectivity of the DBR. DBRs can be made of any two transparent materials with an index contrast, including traditional semiconductors,[2−5] metal-oxides,[6,7] chalcogenides,[8−10] fluorides, and combinations thereof.[11−13]

The choice of materials for a DBR can depend on several factors such as (1) compatibility of the deposition process with other device materials, (2) adhesion between the layers and to the substrate, (3) environmental safety, (4) reproducibility, (5) required reflectivity, (6) spectral range, and (7) spectral width. To date, various techniques and materials have been used for DBR fabrication depending on the above considerations: SiO_2/Si_xN_y by plasma-enhanced chemical vapor deposition (PECVD),[14] AlAs/GaAs and ZnMgSe/ZnCdSe by molecular beam epitaxy (MBE),[15,16] SiO_2/ZrO_2 by reactive helicon-wave-excited-plasma sputtering (R-HWPS) method,[17] ZnO/MgO by RF sputtering,[18] TiO_2/SiO_2 by electron-beam evaporation,[19,20]

Received: September 23, 2014
Accepted: December 16, 2014
Published: December 16, 2014

DOI: 10.1021/am506531p
ACS Appl. Mater. Interfaces 2015, 7, 474−481

and GeSbSe thin films grown at different evaporation angles by thermal evaporation.[21]

Thermal evaporation has the benefit of being a relatively gentle deposition technique because material is deposited on the substrate with comparatively low kinetic energy, without introducing plasma in the chamber or corrosive chemical reactions. Thermal evaporation is therefore suitable for deposition on more delicate materials such as organics. For example, high quality organic microcavities were fabricated by thermally evaporating tellurium oxide (TeO_x) and lithium fluoride (LiF) DBRs on top of fluorescent organic thin films.[14,22]

A common combination of materials for thermally evaporating DBRs is zinc sulfide (ZnS) and magnesium fluoride (MgF_2).[12,23−25] ZnS serves as the high refractive index material with $n_H = 2.38$ at $\lambda = 550$ nm,[26] and MgF_2 as the low refractive index material with $n_L = 1.37$ at $\lambda = 550$ nm.[26] According to eq 1, a DBR made of only six pairs of MgF_2/ZnS on a glass substrate ($n_s = 1.5$) can produce a reflectivity $R = 99.2\%$ at $\lambda_c = 550$ nm, making such mirrors attractive in photonics applications.[24] In practice, careful temperature control is required in order to obtain optical quality MgF_2/ZnS DBRs with good adhesion between the layers and to the substrate. For MgF_2, the substrate needs to be heated to approximately 200 °C[27] to prevent delamination of the layer, whereas for ZnS, the substrate should be held at room temperature.[28] These constraints increase fabrication time because of the time required to heat or cool the substrate in vacuum, and the relatively high temperatures of the MgF_2 deposition can damage soft materials, by pyrolysis, re-evaporation, or uncontrolled annealing.

Here, we demonstrate the design and fabrication of mechanically stable, highly reflecting DBRs based on the combination of thermally evaporated CaF_2 and ZnS layers. We chose these materials for their large refractive index contrast and because CaF_2, like ZnS, can be deposited on substrates that are at room temperature. Both materials have been studied and reported on extensively for a variety of thin film deposition techniques and substrate conditions. Thin films of CaF_2 can be grown via atomic layer deposition[29,30] or molecular beam epitaxy,[31,32] but these approaches require high temperature. Deposition of CaF_2 without heating the substrate was reported using electron beam evaporation,[13] however this technique is a high energy method, unsuitable for deposition on soft materials. Thermal evaporation of CaF_2 thin films was reported at different substrate temperatures, including room temperature.[33]

Single layers of ZnS have been deposited using a number of techniques including chemical bath deposition,[34,35] spray pyrolysis,[36] sputtering,[37] and electron beam evaporation;[38] however, for multilayered coatings, thermal evaporation appears to have been applied most extensively.[12,24,25,28,39] Consequently, we chose to thermally evaporate CaF_2 and ZnS without substrate heating, in order to form multilayer structures via a low-energy process. To the best of our knowledge, no previous reports have been published on deposition of CaF_2 and ZnS together to obtain DBR structures.

Our design goal for the DBR growth was to achieve reflectivity exceeding 99% with a minimum number of layers for a center wavelength of $\lambda_c = 550$ nm. ZnS is the high index material, with $n_H = 2.38$, and CaF_2 is the low index material, with $n_L = 1.43$. The target thicknesses of the CaF_2 and ZnS layers are 96 and 58 nm, respectively. According to eq 1, the reflectivity will exceed $R = 99.5\%$ for DBRs having at least seven pairs (i.e., at least 14 layers). By changing the thicknesses of the layers, these structures can be resonantly tuned to wavelengths throughout the visible spectrum, and hence can be useful for thin film microcavity lasers and next-generation photonic devices.

2. EXPERIMENTAL SECTION

Multilayered Coating. DBRs were grown in a Nano 36 vacuum thermal evaporation system by K.J. Lesker. The system has two thermal sources, which enabled sequential deposition of different materials in a single vacuum cycle. During deposition, thickness and deposition rate were monitored and maintained using an Inficon SQC-310C rate controller and quartz crystal monitors. The base pressure of the evaporator was 3×10^{-7} Torr.

DBR coatings were deposited on thoroughly cleaned double-side polished glass microscope slides. The cleaning procedure was as follows. First, the substrates were sonicated for 5 min in a Micro-90 solution (1% concentration in water), then twice with deionized water, twice with acetone, and then soaked for 10 min in boiling isopropyl alcohol. The substrates were then dried in a stream of nitrogen and treated with oxygen plasma, which served to activate the surface and to promote adhesion before being introduced into the evaporator.

Before growing DBRs, it was necessary to calibrate the crystal monitors for each material. First, single layers of MgF_2, CaF_2, and of ZnS were deposited on glass substrates. Then, the thickness of the layers was measured using a profilometer (Veeco, Dektak 150), ellipsometer (Nanofilm), and a high-resolution scanning electron microscopy (HR-SEM, Zeiss 982) instrument.

To fabricate multilayered structures, we used the two thermal sources of the evaporator and deposited high and low refractive index layers sequentially on clean substrates. Most DBR coatings were composed of CaF_2 and ZnS and consequently were deposited without substrate heating. For comparison purposes, a few DBRs composed of MgF_2 and ZnS were also deposited, with substrate heating (120 °C) or without. For all DBRs that were grown, the center wavelength was chosen to be $\lambda_c = 550$ nm, and the thickness of each layer was chosen to be a quarter wavelength ($d_i = \lambda_c/4n_i$), as required to satisfy the DBR Bragg condition, namely, 100 nm for MgF_2, 96 nm for CaF_2, and 58 nm for ZnS.

To form DBRs, we repeated the deposition of the high and low refractive index layers as described previously. For the CaF_2/ZnS DBRs, first, a single pair composed of one layer of CaF_2 and one layer of ZnS was grown and tested. Then, DBRs composed of six and seven pairs of CaF_2 and ZnS layers were grown (Figure 1). Finally, a complete optical microcavity resonator was deposited that consisted of two 6-pair CaF_2/ZnS DBR coatings and a CaF_2 spacer layer separated between them. The thickness of the spacer was grown to be d = 385 nm, which corresponds to one wavelength of path length at the center wavelength of the mirrors ($d = \lambda_c/n$), with $\lambda_c = 550$ nm and $n = 1.43$

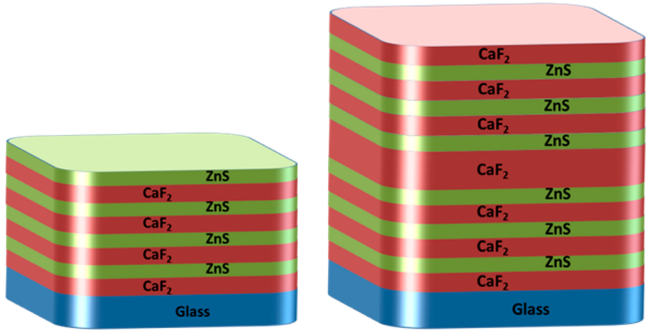

Figure 1. Schematic of a DBR structure (left) and a microcavity resonator structure (right). The structures are composed of alternating CaF_2 and ZnS thin films on a glass substrate.

DOI: 10.1021/am506531p
ACS Appl. Mater. Interfaces 2015, 7, 474−481

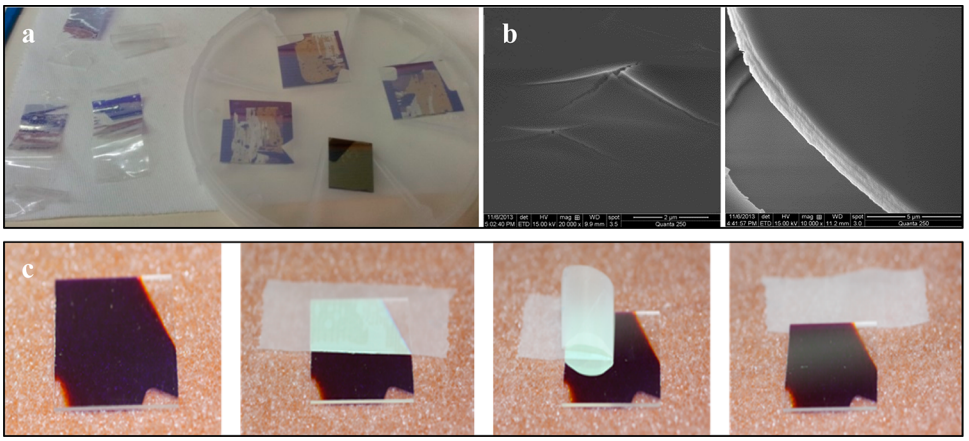

Figure 2. Application of the "Scotch-tape test" to a MgF_2/ZnS DBR (a) resulted in delamination of the layers. Mechanical instability was also observed without applyning the "Scotch-tape test", as shown in the SEM images (b). In contrast, no delamination was observed for the CaF_2/ZnS DBR (c), demonstrating the good adhesion between the CaF_2 and ZnS layers and between them and the substrate.

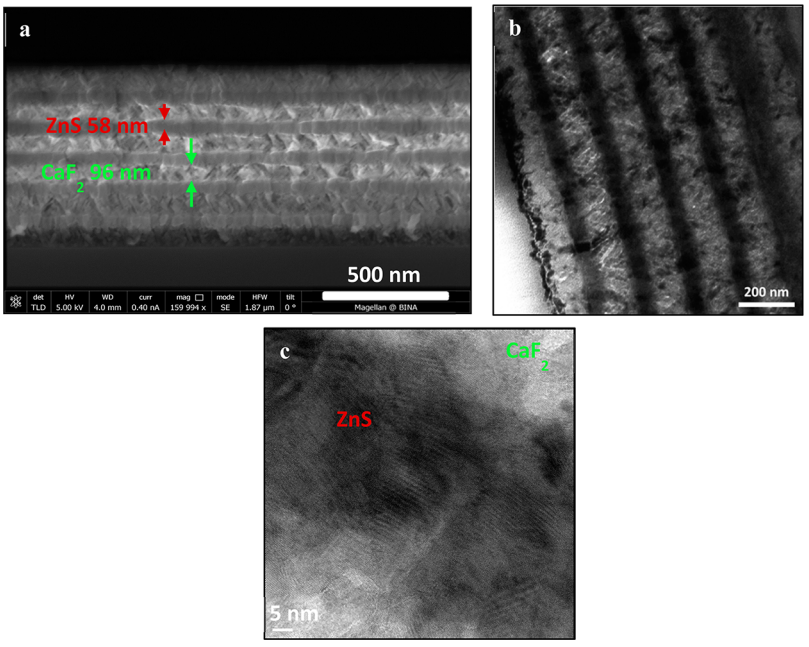

Figure 3. Electron microscope cross-sectional images of a multilayered DBR structure composed of six pairs of CaF_2 and ZnS. In the HR-SEM image (a), the different layers are marked by arrows, with green and red representing CaF_2 and ZnS layers, respectively. In the TEM image (b), the bright bands correspond to CaF_2 and the dark bands to ZnS. The HRTEM image (c) of the ZnS and CaF_2 layers suggests a more gradual transition in composition across the interfaces than shown by HR-SEM and regular TEM in panels a and b.

for CaF_2. For the MgF_2/ZnS DBRs, six pairs of MgF_2 and ZnS layers were grown.

For all materials, the deposition rate was set to be 1 Å/s by regulating the electrical current passing through the evaporation source. The materials were outgassed before evaporation. All depositions were performed at a pressure below 5×10^{-6} Torr.

To characterize the structures, we used high-resolution scanning electron microscopy (HR-SEM, Zeiss 982), focused ion beam (FIB, Helios 600), X-ray diffraction (XRD, Rigaku Smartlab), transmission electron microscopy (TEM, JEM 1400), and high-resolution TEM (HR-TEM, JEOL-2100) with a Noran System Six energy dispersive X-ray spectrometry (EDS) system for elemental analysis. Optical transmission spectra were obtained for thin film, DBR, and microcavity samples using a spectrophotometer (Cary 100 UV−vis, Agilent Technologies Inc.), whereas reflection spectra were measured in a home-built optical scanner.[40] Measurements were taken at normal incidence.

Organic Film Fabrication. To characterize the effects of coating such DBRs onto soft materials, with and without substrate heating, thin films of fluorescent organic dye were prepared and then coated with DBRs. The films were composed of poly(methyl methacrylate) (PMMA) doped with the dye rhodamine 6G (R6G). The PMMA and R6G were dissolved in dimethylformamide (DMF) in a ratio of 99.95% polymer to 0.05% dye (weight/weight). Then, the solution was spin-cast onto glass substrates, at 2000 rpm for 90 s with a ramp acceleration of 1000 rpm/s (using a Headway Research PWM32 spin-coater), yielding films of approximately 1 μm thickness, as measured by profilometry.

After the organic films were prepared, DBR coatings of MgF_2/ZnS and CaF_2/ZnS were deposited on top of the layers, with and without substrate heating, respectively, as described above in the DBR fabrication section. Photoluminescence (PL) spectra were then measured and compared using a micro-PL setup (HORIBA Scientific LabRAM HR) in air at room temperature. The samples were excited

DOI: 10.1021/am506531p
ACS Appl. Mater. Interfaces 2015, 7, 474−481

by a laser with an excitation wavelength of λ_{ex} = 405 nm, and the fluorescence signal was collected with high spectral resolution.

3. RESULTS AND DISCUSSION

The adhesion of the DBR coatings was examined by performing the "Scotch-tape test", which is a commonly used method for ascertaining the adhesion strength of thin films to substrates.[41−45] In the test, we applied adhesive tape to the surface of the DBR coating and slowly pulled off the tape by hand. The coating fails the test if any of it delaminates from the substrate and remains on the adhesive tape.

For the MgF_2/ZnS DBR samples that were grown at room temperature, adhesive tape easily separated the upper MgF_2 and ZnS layers from the lower layers and from the glass substrate (Figure 2a). For these coatings, delamination and cracking occurred occasionally even without applying the "Scoth-tape test" (Figure 2b). The instability of the MgF_2/ZnS coatings is likely due to high surface tension between the layers, and it can be mitigated by heating the substrate during deposition to 120 °C, but this solution renders MgF_2/ZnS incompatible for application on soft materials. For CaF_2/ZnS coatings, strong adhesion was observed between the CaF_2 and ZnS layers and with the glass substrate. Even after repeating the "Scotch-tape test" multiple times, the tape remained clean and no damage to the DBR coatings was apparent (Figure 2c).

The "Scotch-tape test" was effective in demonstrating the stark difference in adhesion between CaF_2/ZnS and MgF_2/ZnS DBR coatings when both were grown without substrate heating. In addition to the "Scotch-tape test", which was essentially qualitative, we quantified the force of adhesion between the Scotch tape and the different samples and found that the force to pull the tape from a CaF_2/ZnS DBR is 5 times greater than from the MgF_2/ZnS DBR (Figure S1 and Table S1; see the Supporting Information).

The structure of the DBRs was determined by high-resolution scanning electron microscopy (HR-SEM). Figure 3a shows a cross-sectional image of the alternating layers of CaF_2 and ZnS in the DBR structure. The layers appear to be distinct, smooth, and homogeneous. We measured the thicknesses of the layers to be 96 nm ±1.6% (±1.54 nm) and 58 nm ±2.8% (±1.62 nm) for the CaF_2 and ZnS layers, respectively. The thicknesses of the deposited films are quite consistent. We then performed transmission electron microscopy (TEM) to observe the detailed microstructure. Figure 3b shows the cross-sectional TEM image of the DBR structure with the alternating layers of CaF_2 and ZnS. In the TEM image, the bright bands represent CaF_2 and the dark bands represent ZnS. The image shows that the layers are distinct and well separated, with nanovoids observed within each layer, indicating a smooth yet nanoporous structure.

The interface between the ZnS and CaF_2 layers is shown in the HR-TEM image of Figure 3c. The image indicates the presence of a small transition region between the layers in which the composition is changing between being only CaF_2 to only ZnS. The HR-TEM image suggests that the transition occurs more gradually than shown in the HR-SEM and regular TEM images.

To gain greater insight into the composition of the layers, we performed XRD on single layer and multilayered structures. The crystalline phases of CaF_2 and ZnS are shown in Figure 4 for a six-pair DBR. The structures were polycrystalline in all cases. A cubic phase of CaF_2 (fcc) with estimated lattice constants $a = b = c$ = 5.463 Å, and a hexagonal phase of ZnS

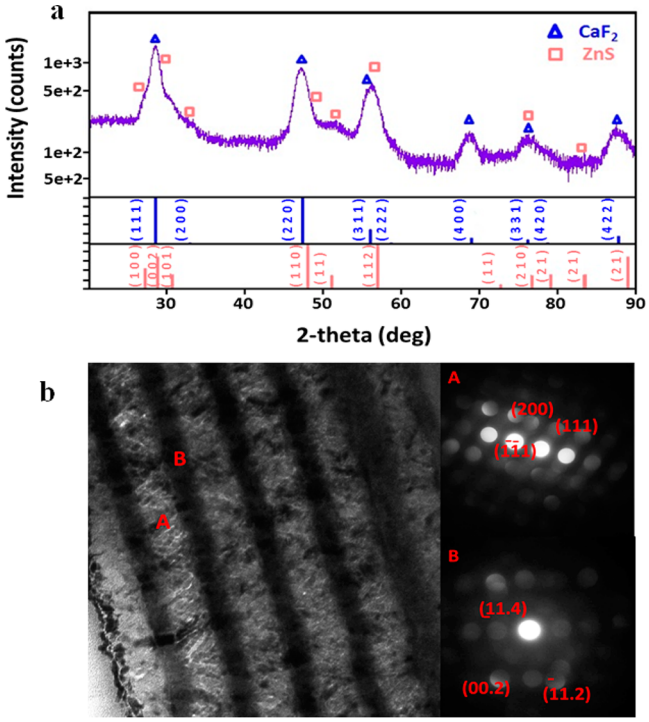

Figure 4. XRD analysis (a) and indexed microbeam electron diffraction patterns (b) demonstrate the presence of (A) cubic CaF_2 and (B) hexagonal ZnS phases. The lattice parameters are cubic $a = b = c$ = 5.463 Å, and hexagonal with $a = b$ = 3.83 Å, c = 6.26 Å for the CaF_2 and ZnS layers, respectively.

(wurtzite) with estimated lattice constants $a = b$ = 3.83 Å, c = 6.26 Å were determined. These results correspond to standard lattice parameters.[46] The XRD pattern for the CaF_2/ZnS DBR of Figure 4a exhibits pristine phases for both CaF_2 and ZnS. No additional peaks or secondary phases were observed in the combined phases of the CaF_2/ZnS DBR, which confirms that lattice diffusion did not occur during fabrication of the composite system. Moreover, no impurity peaks were found in the XRD pattern. The crystallinity of the DBR layers was further supported by selected area electron diffraction (Figure S2; see the Supporting Information), and by microbeam electron diffraction performed with a convergent electron probe below 7 nm (Figure 4b). The diffraction patterns, obtained from both the CaF_2 and ZnS layers (A and B in Figure 4b, respectively), demonstrate the presence of cubic CaF_2 and hexagonal ZnS phases, in agreement with the XRD results.

We then fabricated a complete microcavity structure from CaF_2 and ZnS, and characterized its morphology by HR-SEM and TEM (Figure 5). In the HR-SEM cross-sectional image (Figure 5a), the entire microcavity structure can be seen, which consists of top and bottom DBRs, and a CaF_2 spacer in between them. Each DBR has six pairs of CaF_2 and ZnS layers. From the HR-SEM image, the thickness of the CaF_2 cavity spacer layer was determined to be approximately 395 nm ±5% (±20 nm), which is in agreement to the target value of d = 385 nm, as described in the Experimental Section. The TEM image (Figure 5b) shows the region of the microcavity structure in the vicinity of the CaF_2 spacer. The dark bands represent ZnS layers and the bright bands represent CaF_2. From the electron microscopy images, we see that the thicker CaF_2 spacer layer exhibits bigger pores compared to the DBR layers, and is also less smooth. These characteristics affect the morphology of the

DOI: 10.1021/am506531p
ACS Appl. Mater. Interfaces 2015, 7, 474−481

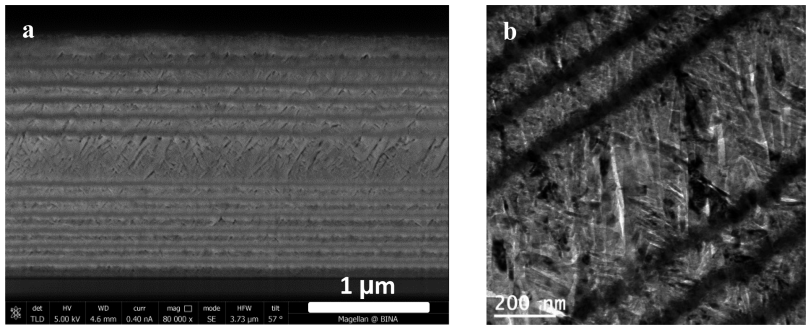

Figure 5. HR-SEM (a) and TEM (b) cross-sectional images of a CaF_2/ZnS microcavity structure. The HR-SEM image (a) shows the entire structure of 25 layers: 12 for each DBR and the CaF_2 spacer layer between them. The TEM image (b) is focused on the CaF_2 spacer. The bright and dark bands represent the CaF_2 and ZnS layers, respectively.

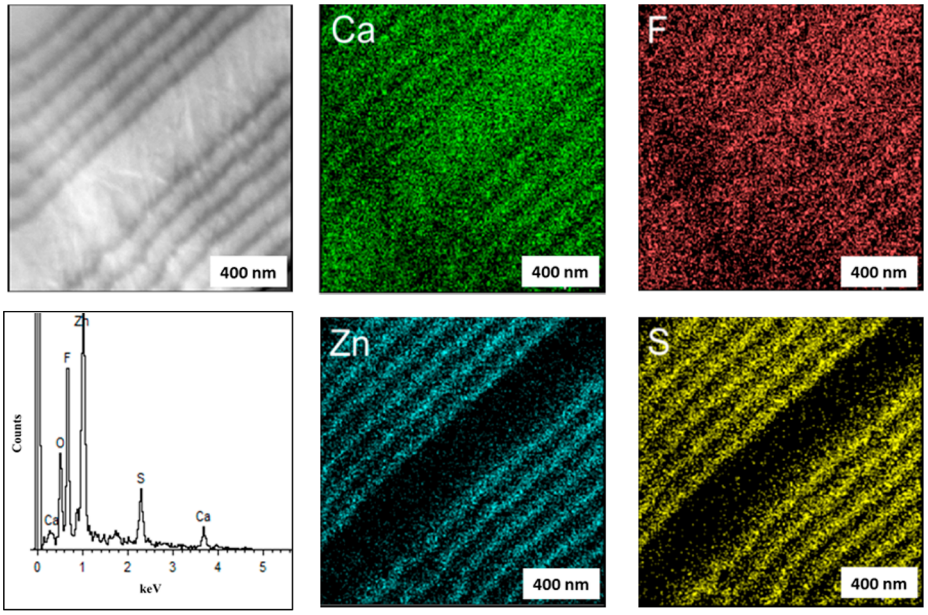

Figure 6. EDX analysis and mapping from a TEM cross section of the microcavity structure show the presence of the elements that compose the structure (Ca - green, F - red, Zn - blue, and S - yellow) and their distribution across the layers.

top DBR coating, which also appears to be rougher than the bottom DBR. Nevertheless, the layers in the microcavity structure are distinct and well-separated.

To further ascertain the composition of the layers, we performed energy-dispersive X-ray (EDX) analysis on the microcavity structure. EDX indicated the presence of Ca, F, Zn, and S elements within the multilayered stack and also showed no trace of an impurity. The dispersion of the elements over the layers is shown in the mapping EDX analysis (Figure 6). The dispersion confirms that the two different layers are indeed composed of CaF_2 and ZnS, with good separation between them.

Next, we characterized the optical properties of the thermally evaporated CaF_2/ZnS DBR and microcavity structures. Figure 7 shows the transmission curves versus wavelength. The transmission spectrum of a CaF_2 (100 nm) layer is shown in Figure 7a, which exhibited a nearly constant transmittance of ~95% from 300 to 800 nm. The transmission spectrum of a thin (50 nm) ZnS layer is shown in Figure 7b. The transmittance increases for longer wavelengths and reaches a maximum of 85% at 800 nm. In Figure 7c, the transmission spectra are shown for multilayered structures composed of one pair and seven pairs of CaF_2/ZnS. For one pair of CaF_2/ZnS, the transmission decreases to almost 70% in the wavelength range from 500 to 800 nm, because of the optical interference between the CaF_2 and ZnS layers. The seven-pair structure of CaF_2/ZnS exhibited a typical transmission curve of a DBR. In the wavelength range between 500 and 600 nm, the transmission is T = 0.5%. This range of wavelengths is where the structure is most reflective. As mentioned above, the layer thicknesses were chosen to produce a maximum reflectivity at a center wavelength of 550 nm. At λ_c = 550 nm, the measured reflectance is R = 99.3% (Figure S3; see the Supporting Information for the full curve), which is close to the predicted value of R = 99.5%. From the reflection and transmission measurements, we can quantify the absorption and scattering losses at λ_c = 550 nm to be A = 0.2% ($R + T + A$ = 100%). The stopband of the DBR has a full width at half-maximum (fwhm) of 204 nm. A theoretical calculation predicts a stopband with a fwhm = 176 nm for the same center wavelength. The deviation of 8% can be attributed to variation in the refractive index of the layers versus wavelength, which was not accounted for in the calculation.

The transmission curve for a complete microcavity structure is shown in Figure 7d. The thickness of the CaF_2 spacer layer between the two DBRs enables a specific wavelength to be

DOI: 10.1021/am506531p
ACS Appl. Mater. Interfaces 2015, 7, 474−481

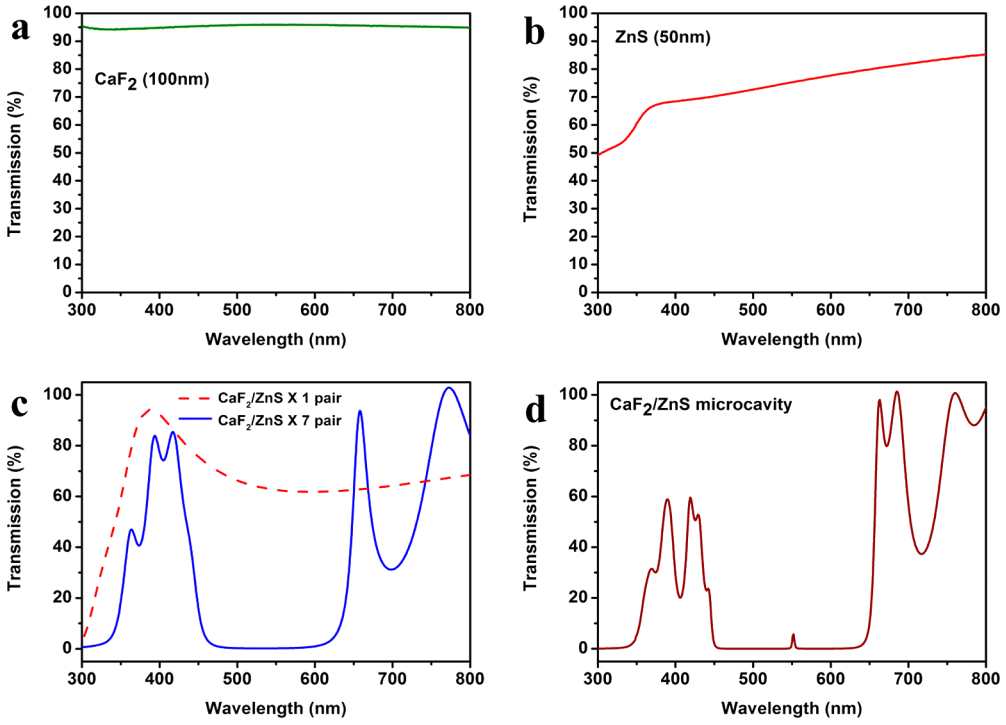

Figure 7. Optical transmission was measured versus wavelength for thin films of 100 nm of CaF_2 (a), and 50 nm of ZnS (b), for multilayered structures (c) of 1 pair and 7 pairs of CaF_2 and ZnS layers, shown as dashed-red and blue lines, respectively, and for a complete optical microcavity (d) containing 25 layers. From the width of the cavity resonance peak, a resonator quality factor of Q = 167 was derived.

resonantly transmitted, which in this case is λ = 553 nm. The fwhm of the transmitssion peak is observed to be $\Delta\lambda$ = 3.33 nm. From the fwhm and the wavelength of the transmission peak, the quality factor (Q) of the microcavity can be calculated using the equation that $Q = \lambda/\Delta\lambda$, which in our case gives Q = 167. Although an increase in transmission is observed at λ = 553 nm, typically one would expect values approaching 99%, given the mirrors are highly reflecting and low loss in this wavelength range. The reason we observed only a modest increase in transmission can likely be attributed to inhomogeneity in the spacer layer thickness across the sample, as was observed in the HR-SEM image of Figure 5a. This spread leads directly to a distribution in the resonant transmission wavelength. Because the transmission measurement performed in the spectrophotometer samples this distribution simultaneously, the result is a blurring of the observed resonant transmission wavelength, a corresponding increase in the fwhm of the transmission resonance, and also a pronounced reduction in the peak transmission.

To illustrate the beneficial effects of growing CaF_2/ZnS DBR coatings without substrate heating, PL was measured for a fluorescent organic thin film of PMMA:R6G and then for an identically prepared PMMA:R6G film with a six-pair CaF_2/ZnS DBR coated on top. A laser with an excitation wavelength of λ_{ex} = 405 nm was used to excite the samples, and PL spectra were obtained by exciting the samples and collecting signal from the substrate side of the structures. As shown in Figure 8, the PL spectrum of the DBR coated film was nearly twice as intense as the thin film by itself, because the reflection from the DBR causes twice as much light to be collected. It is also apparent that the process of coating the CaF_2/ZnS DBR did not quench the fluorescence of the underlying PMMA:R6G film, because if such damage had occurred then less enhancement would have been observed. For comparison, an identically prepared

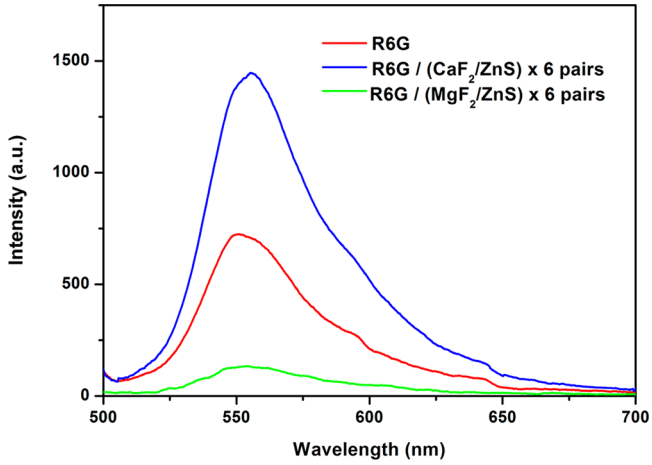

Figure 8. Photoluminescence spectra were obtained from three samples: a thin film of the fluorescent dye Rhodamine 6G doped into a PMMA matrix without a DBR coating on top (red curve), and identically prepared R6G:PMMA films with a CaF_2/ZnS DBR grown on top (blue curve), and with a MgF_2/ZnS DBR on top (green curve). The CaF_2/ZnS structure, which does not involve substrate-heating, shows nearly twice the signal of the uncoated film, due to reflection from the DBR. In contrast, the MgF_2/ZnS based structure, which required substrate heating to 120 °C, showed a decrease in fluoresence intensity due to thermally induced damage.

PMMA:R6G layer was coated with a MgF_2/ZnS DBR that was grown with substrate heating to 120 °C. As shown in Figure 8, the PL intensity decreased in this case by 5.5 times relative to the uncoated film, and by 11 times compared to the CaF_2/ZnS DBR. These results illustrate the instability of some organic films to higher temperatures and also the ability to

DOI: 10.1021/am506531p
ACS Appl. Mater. Interfaces 2015, 7, 474−481

overcome this problem by depositing CaF_2/ZnS DBRs without substrate heating.

4. CONCLUSION

Mechanically stable, reproducible, and highly reflecting DBRs were realized based on thermally evaporated CaF_2 and ZnS multilayered coatings. These two materials were found to adhere well to the substrate and to each other even though the deposition was performed on an unheated substrate. The layers are distinct and well-separated, as was shown in HR-SEM and TEM images. Due to the large refractive index contrast, CaF_2/ZnS DBRs exhibited excellent optical characteristics in terms of transmission stop band, high reflectivity, and low optical loss. This room temperature process, which results in stable high-reflectivity structures, could be useful for fabrication of photonic devices based on organics or other nanomaterials such as organic vertical cavity surface emitting lasers (VCSELs)[47−49] or perovskite VCSELs,[50] where it is beneficial to grow a DBR directly on top of a soft film, and simultaneously preserve the optical properties of the active layer.

■ ASSOCIATED CONTENT

Supporting Information

Measurements of the force of adhesion between adhesive tape and several coatings are described. The tensile strength test apparatus is shown in Figure S1, and the results of the testing are summarized in Table S1. Selected area electron diffraction patterns taken for a CaF_2/ZnS DBR are shown in Figure S2. The reflection spectrum of a CaF_2/ZnS DBR is shown in Figure S3. This material is available free of charge via the Internet at http://pubs.acs.org.

■ AUTHOR INFORMATION

Corresponding Author

*Y. R. Tischler. E-mail: yaakov.tischler@biu.ac.il. Tel: 972-3-7384514. Fax: 972-3-738-4053.

Notes

The authors declare no competing financial interest.

■ ACKNOWLEDGMENTS

This research was supported by the Israel Science Foundation (ISF). We are grateful to Gili Cohen-Taguri for her help with XRD measurements, to Luba Burlaka for her help with TEM imaging and EDX analysis, to Dr. Judith Grinblat for her help with the HR-TEM, to Joanna Chen for her help with the thermal evaporation system, to Paniel Miron for help with his tensile tester machine, and to Prof. Arie Zaban and David Keller for help using their optical scanner.

■ REFERENCES

(1) Sheppard, C. J. R. Approximate Calculation of the Reflection Coefficient from a Stratified Medium. *J. Eur. Opt. Soc., Part A* **1995**, *4*, 665.

(2) Mukaihara, T.; Ohnoki, N.; Hayashi, Y.; Hatori, N.; Koyama, F.; Iga, K. Polarization Control of Vertical-Cavity Surface Emitting Lasers Using a Birefringent Metal/Dielectric Polarizer Loaded on Top Distributed Bragg Reflector. *IEEE J. Sel. Top. Quantum Electron.* **1995**, *1*, 667−673.

(3) Tsuda, S.; Knox, W. H.; de Souza, E. A.; Jan, W. Y.; Cunningham, J. E. Low-Loss Intracavity AlAs/AlGaAs Saturable Bragg Reflector for Femtosecond Mode Locking in Solid-State Lasers. *Opt. Lett.* **1995**, *20*, 1406−1408.

(4) Brand, S.; Kaliteevski, M. A.; Abram, R. A. Optical Tamm States above the Bulk Plasma Frequency at a Bragg Stack/Metal Interface. *Phys. Rev. B* **2009**, *79*, 085416-1−085416-4.

(5) MacDougal, M. H.; Dapkus, P. D.; Pudikov, V.; Hanmin, Z.; Yang, G.-M. Ultralow Threshold Current Vertical-Cavity Surface-Emitting Lasers with AlAs Oxide-GaAs Distributed Bragg Reflectors. *IEEE Photonics Technol. Lett.* **1995**, *7*, 229−231.

(6) Choi, S. Y.; Mamak, M.; von Freymann, G.; Chopra, N.; Ozin, G. A. Mesoporous Bragg Stack Color Tunable Sensors. *Nano Lett.* **2006**, *6*, 2456−2461.

(7) Kahl, M.; Thomay, T.; Kohnle, V.; Beha, K.; Merlein, J.; Hagner, M.; Halm, A.; Ziegler, J.; Nann, T.; Fedutik, Y.; Woggon, U.; Artemyev, M.; Pérez-Willard, F.; Leitenstorfer, A.; Bratschitsch, R. Colloidal Quantum Dots in All-Dielectric High-Q Pillar Microcavities. *Nano Lett.* **2007**, *7*, 2897−2900.

(8) Tawara, T.; Arita, M.; Uesugi, K.; Suemune, I. MOVPE Growth of ZnSe/ZnS Distributed Bragg Reflectors on GaAs (1 0 0) and (3 1 1)B Substrates. *J. Cryst. Growth* **1998**, *184−185*, 777−782.

(9) Takehiko, T.; Munetaka, A.; Katsuhiro, U.; Ikuo, S. ZnSe/ZnS Distributed Bragg Reflectors in the Blue Region Grown on (311)B GaAs Substrates. *Jpn. J. Appl. Phys.* **1997**, *36*, 6672.

(10) Kovalev, V. I.; Kuznetsov, P. I.; Zhitov, V. A.; Zakharov, L. Y.; Rukovishnikov, A. I.; Khomich, A. V.; Yakushcheva, G. G.; Gaponenko, S. V. Spectral Ellipsometry of Multilayer ZnS/ZnSe Heterostructures. *J. Appl. Spectrosc.* **2002**, *69*, 298−304.

(11) Liu, X.; Li, H.; Song, C.; Liao, Y.; Tian, M. Microcavity Organic Laser Device under Electrical Pumping. *Opt. Lett.* **2009**, *34*, 503−505.

(12) Kedawat, G.; Srivastava, S.; Jain, V. K.; Kumar, P.; Kataria, V.; Agrawal, Y.; Gupta, B. K.; Vijay, Y. K. Fabrication of Artificially Stacked Ultrathin ZnS/MgF2 Multilayer Dielectric Optical Filters. *ACS Appl. Mater. Interfaces* **2013**, *5*, 4872−4877.

(13) Lei, C.; Rogers, T. J.; Deppe, D. G.; Streetman, B. G. ZnSe/CaF2 Quarter-Wave Bragg Reflector for the Vertical-Cavity Surface-Emitting Laser. *J. Appl. Phys.* **1991**, *69*, 7430−7434.

(14) Adawi, A. M.; Cadby, A.; Connolly, L. G.; Hung, W. C.; Dean, R.; Tahraoui, A.; Fox, A. M.; Cullis, A. G.; Sanvitto, D.; Skolnick, M. S.; Lidzey, D. G. Spontaneous Emission Control in Micropillar Cavities Containing a Fluorescent Molecular Dye. *Adv. Mater.* **2006**, *18*, 742−747.

(15) Ustinov, V. M.; Maleev, N. A.; Zhukov, A. E.; Kovsh, A. R.; Egorov, A. Y.; Lunev, A. V.; Volovik, B. V.; Krestnikov, I. L.; Musikhin, Y. G.; Bert, N. A.; Kop'ev, P. S.; Alferov, Z. I.; Ledentsov, N. N.; Bimberg, D. InAs/InGaAs Quantum Dot Structures on GaAs Substrates Emitting at 1.3 μm. *Appl. Phys. Lett.* **1999**, *74*, 2815−2817.

(16) Peiris, F. C.; Lee, S.; Bindley, U.; Furdyna, J. K. ZnMgSe/ZnCdSe and ZnMgSe/ZnSeTe Distributed Bragg Reflectors Grown by Molecular Beam Epitaxy. *J. Appl. Phys.* **1999**, *86*, 719−724.

(17) Chichibu, S. F.; Ohmori, T.; Shibata, N.; Koyama, T. Dielectric SiO_2/ZrO_2 Distributed Bragg Reflectors for ZnO Microcavities Prepared by the Reactive Helicon-Wave-Excited-Plasma Sputtering Method. *Appl. Phys. Lett.* **2006**, *88*, 161914-1−161914-3.

(18) Huang, Y. S.; Chang, C. C.; Lee, J. W.; Lee, Y. C.; Huang, C. C.; Kwun, Z.; Tiong, K. K. Optical Studies in Distributed Bragg Reflectors Built from ZnO/MgO Multilayer Films. *Phys. Scr.* **2013**, *2013*.

(19) de Denus-Baillargeon, M.-M.; Schmitt, T.; Larouche, S.; Martinu, L. Design and Fabrication of Stress-Compensated Optical Coatings: Fabry-Perot Filters for Astronomical Applications. *Appl. Opt.* **2014**, *53*, 2616−2624.

(20) Martiradonna, L.; Carbone, L.; De Giorgi, M.; Manna, L.; Gigli, G.; Cingolani, R.; De Vittorio, M. High Q-Factor Colloidal Nanocrystal-based Vertical Microcavity by Hot Embossing Technology. *Appl. Phys. Lett.* **2006**, *88*, 181108-1−181108-3.

(21) Martin-Palma, R. J.; Torres-Costa, V.; Pantano, C. G. Distributed Bragg Reflectors Based on Chalcogenide Glasses for Chemical Optical Sensing. *J. Phys. D: Appl. Phys.* **2009**, *42*, 055109.

(22) Anni, M.; Gigli, G.; Cingolani, R.; Patanè, S.; Arena, A.; Allegrini, M. Organic M Cavities Based on Thermally Evaporated TeOx-LiF Distributed Bragg Reflectors. *Appl. Phys. Lett.* **2001**, *79*, 1381−1383.

DOI: 10.1021/am506531p
ACS Appl. Mater. Interfaces 2015, 7, 474−481

(23) Zhao, X.; Wu, Z.; Liang, S.; Hou, X. Optimal Design and Experimental Realization of DBR-Metal Microcavity Organic Lasers. *Semicond. Lasers Appl. IV* **2010**, *7844*, 78441B-1−78441B-7.
(24) Soto, D.; Perales, F.; Lifante, G.; Heras, C. d. l. Evolution of the Optical and Structural Properties in ZnS/MgS_2 Multilayers as the Number of Layers Increases. *J. Phys. D: Appl. Phys.* **2009**, *42*, 215402.
(25) Perales, F.; Soto, D.; de las Heras, C. Dependence of Optical and Structural Properties of ZnS and MgF_2 Multilayers as a Function of the Number of Layers. *Thin Solid Films* **2010**, *518*, 4221−4224.
(26) Bass, M. *Handbook of Optics*; McGraw-Hill: New York, 2010.
(27) Yu, H.; Qi, H.; Cui, Y.; Shen, Y.; Shao, J.; Fan, Z. Influence of Substrate Temperature on Properties of MgF_2 Coatings. *Appl. Surf. Sci.* **2007**, *253*, 6113−6117.
(28) Salleh, S.; Chik, A.; Dalimin, M. N.; Salleh, M. M.; Rutt, H. N. Surface Roughness of Thermally Evaporated ZnS Optical Waveguides. In *Asian Conference on Sensors and the International Conference on new Techniques in Pharmaceutical and Biomedical Research*, Kuala Lumpur, Malaysia, September 5−7, 2005; IEEE: New York, 2005; pp 229−232.
(29) Pilvi, T.; Arstila, K.; Leskelä, M.; Ritala, M. Novel ALD Process for Depositing CaF_2 Thin Films. *Chem. Mater.* **2007**, *19*, 3387−3392.
(30) Putkonen, M.; Szeghalmi, A.; Pippel, E.; Knez, M. Atomic Layer Deposition of Metal Fluorides through Oxide Chemistry. *J. Mater. Chem.* **2011**, *21*, 14461−14465.
(31) Mattoso, N.; Mosca, D. H.; Mazzaro, I.; Teixeira, S. R.; Schreiner, W. H. The Epitaxial Growth of Evaporated Cu/CaF_2 Bilayers on Si(111). *J. Appl. Phys.* **1995**, *77*, 2831−2833.
(32) Harrison, T. R.; Mankiewich, P. M.; Dayem, A. H. Thin-Film CaF_2 Inorganic Electron Resist and Optical-Read Storage Medium. *Appl. Phys. Lett.* **1982**, *41*, 1102−1104.
(33) Kaiser, U.; Kaiser, N.; Weiβbrodt, P.; Mademann, U.; Hacker, E.; Müller, H. Structure of Thin Fluoride Films Deposited on Amorphous Substrates. *Thin Solid Films* **1992**, *217*, 7−16.
(34) Cheng, J.; Fan, D.; Wang, H.; Liu, B.; Zhang, Y.; Yan, H. Chemical Bath Deposition of Crystalline ZnS Thin Films. *Semicond. Sci. Technol.* **2003**, *18*, 676.
(35) Roy, P.; Ota, J. R.; Srivastava, S. K. Crystalline ZnS Thin Films by Chemical Bath Deposition Method and Its Characterization. *Thin Solid Films* **2006**, *515*, 1912−1917.
(36) Elidrissi, B.; Addou, M.; Regragui, M.; Bougrine, A.; Kachouane, A.; Bernède, J. C. Structure, Composition and Optical Properties of ZnS Thin Films Prepared by Spray Pyrolysis. *Mater. Chem. Phys.* **2001**, *68*, 175−179.
(37) Mukherjee, C.; Rajiv, K.; Gupta, P.; Sinha, A. K.; Abhinandan, L. Growth and Characterization of High Quality ZnS Thin Films by RF Sputtering. *AIP Conf. Proc.* **2012**, *1451*, 230−232.
(38) Ragachev, A. V.; Yarmolenko, M. A.; Rogachev, A. A.; Gorbachev, D. L.; Zhou, B. Chemical Composition, Morphology and Optical Properties of Zinc Sulfide Coatings Deposited by Low-Energy Electron Beam Evaporation. *Appl. Surf. Sci.* **2014**, *303*, 23−29.
(39) Leftheriotis, G.; Yianoulis, P.; Patrikios, D. Deposition and Optical Properties of Optimised ZnS/Ag/ZnS Thin Films for Energy Saving Applications. *Thin Solid Films* **1997**, *306*, 92−99.
(40) Anderson, A. Y.; Bouhadana, Y.; Barad, H. N.; Kupfer, B.; Rosh-Hodesh, E.; Aviv, H.; Tischler, Y. R.; Ruhle, S.; Zaban, A. Quantum Efficiency and Bandgap Analysis for Combinatorial Photovoltaics: Sorting Activity of Cu-O Compounds in All-Oxide Device Libraries. *ACS Comb. Sci.* **2014**, *16*, 53−65.
(41) Kim, Y.-K.; Min, D.-H. Durable Large-Area Thin Films of Graphene/Carbon Nanotube Double Layers as a Transparent Electrode. *Langmuir* **2009**, *25*, 11302−11306.
(42) Griffith, J. E.; Qiu, Y.; Tombrello, T. A. Ion-Beam-Enhanced Adhesion in the Electronic Stopping Region. *Nucl. Instrum. Methods Phys. Res.* **1982**, *198*, 607−609.
(43) Dini, J. W. *Electrodeposition: The Materials Science of Coatings and Substrates*; Noyes Publications: Park Ridge, NJ, 1993.
(44) Yeh, J.-M.; Weng, C.-J.; Liao, W.-J.; Mau, Y.-W. Anticorrosively Enhanced PMMA−SiO_2 Hybrid Coatings Prepared from the Sol−Gel Approach with MSMA as the Coupling Agent. *Surf. Coat. Technol.* **2006**, *201*, 1788−1795.
(45) Xie, X.; Yu, G.; Liu, N.; Bao, Z.; Criddle, C. S.; Cui, Y. Graphene-Sponges as High-Performance Low-Cost Anodes for Microbial Fuel Cells. *Energy Environ. Sci.* **2012**, *5*, 6862−6866.
(46) Lide, D. R. *Handbook of Chemistry and Physics*, 88th ed.; CRC Press: Boca Raton, FL, 2007−2008.
(47) Bulović, V.; Kozlov, V. G.; Khalfin, V. B.; Forrest, S. R. Transform-Limited, Narrow-Linewidth Lasing Action in Organic Semiconductor Microcavities. *Science* **1998**, *279*, 553−555.
(48) Koschorreck, M.; Gehlhaar, R.; Lyssenko, V. G.; Swoboda, M.; Hoffmann, M.; Leo, K. Dynamics of a High-Q Vertical-Cavity Organic Laser. *Appl. Phys. Lett.* **2005**, *87*, 181108.
(49) Rennie, J.; Ushirogouchi, T.; Hatakoshi, G.-i. Vertical-Cavity Surface-Emitting Lasers Constructed with Alq3 Active Regions Employing a DBR Structure. *Proc. SPIE* **2001**, *4279*, 196−203.
(50) Brehier, A.; Parashkov, R.; Lauret, J. S.; Deleporte, E. Strong Exciton-Photon Coupling in a Microcavity Containing Layered Perovskite Semiconductors. *Appl. Phys. Lett.* **2006**, *89*, 171110-1−171110-3.

DOI: 10.1021/am506531p
ACS Appl. Mater. Interfaces 2015, 7, 474−481